

Substitutional disorder and anion ordering transition in the $(\text{TMTSF})_2(\text{ReO}_4)_{1-x}(\text{ClO}_4)_x$ solid solution

V. Ilakovac,* S. Ravy, K. Boubekeur,† C. Lenoir, P. Batail,† and J. P. Pouget

Laboratoire de Physique des Solides (CNRS URA 02), Université Paris Sud, 91405 Orsay, France

(Received 21 April 1997)

We present an x-ray diffuse scattering study of the anion ordering (AO) transition in the $(\text{TMTSF})_2(\text{ReO}_4)_{1-x}(\text{ClO}_4)_x$ solid solution of quasi-one-dimensional organic conductors and superconductors. As $(\text{TMTSF})_2\text{ReO}_4$ and $(\text{TMTSF})_2\text{ClO}_4$ present AO instabilities at different critical wave vectors [$\mathbf{q}_1 = (\frac{1}{2}, \frac{1}{2}, \frac{1}{2})$ and $\mathbf{q}_2 = (0, \frac{1}{2}, 0)$, respectively] this solid solution allows for the study of the influence of competing interactions on a structural transition. The order parameter of this transition can be characterized by an Ising variable representing the two possible orientations of the ReO_4^- or ClO_4^- anion in cavities delimited by organic TMTSF molecules. Furthermore, the random substitution of the anions shows that these interactions are randomly distributed. The phase diagram of the AO transition has been determined as a function of x . At low temperatures (T) a \mathbf{q}_1 long-range order (LRO) occurs for $x \leq 0.5$ and a \mathbf{q}_2 LRO occurs for $1 \leq x \leq 0.97$, while a short-range order (SRO) appears in the intermediate concentration range. For $0.7 < x < 0.94$ one observes coexistence of \mathbf{q}_1 and \mathbf{q}_2 SRO. The basic features of the (T, x) phase diagram can be accounted for by a mean-field treatment of the Ising model with random interactions. This model, however, fails to reproduce all the details of the phase diagram, such as the x dependence of the critical wave vector. Finally, we discuss the implications of this structural phase diagram on the electronic properties of the solid solution. [S0163-1829(97)02041-9]

I. INTRODUCTION

For more than 15 years, the 2:1 cation radical salts of TMTSF (tetramethyl-tetraselenafulvalenium) and TMTTF (tetramethyl-tetrathiafulvalenium) organic molecules have attracted the attention of physicists and chemists because of the rich phase diagram associated with their quasi-one-dimensional (1D) electronic properties. They are conductors at room temperature. Some of them become superconducting at low temperatures (especially under pressure), but, because of their low electronic dimensionality, the metallic state is generally unstable at low temperatures and atmospheric pressure with respect to different kinds of nonconducting ground states.^{1,2}

$[\text{TMTS}(\text{T})\text{F}]_2\text{X}$ salts crystallize in the triclinic space group $P\bar{1}$. One center of inversion is placed on each anion site, so that *centrosymmetric* anions ($X = \text{PF}_6^-$, AsF_6^- , SbF_6^- , Br^- , etc.) have a unique position in the structure. In these salts, the instability of the metallic state is due to the instability of the 1D electronic system located on the organic stacks (directed along the \mathbf{a} direction). Several kinds of instabilities leading to spin-density-wave³ (SDW) and spin-peierls⁴ (SP) ground states or to superconductivity⁵ are observed in salts with centrosymmetric anions. Because of their lack of inversion symmetry, *noncentrosymmetric* anions ($X = \text{ReO}_4^-$, ClO_4^- , BF_4^- , NO_3^- , SCN^- , etc.) can take at least two equivalent positions in the $P\bar{1}$ structure. They can point toward the Se(S) atom of one of the two symmetry related neighboring TMTS(T)F organic molecule [Fig. 1(a)]. At room temperature, these anions are disordered. At low temperature they order⁶ in such a way that neighboring anions align or alternate their orientation. For example, in $(\text{TMTSF})_2\text{ReO}_4$, the orientation of the ReO_4^- alternates in

the three crystallographic directions below $T_{\text{AO}} = 176$ K.⁷ This order is thus characterized by the reduced wave vector $\mathbf{q}_1 = (1/2, 1/2, 1/2)$. In $(\text{TMTSF})_2\text{ClO}_4$, at a temperature as low as $T_{\text{AO}} = 24$ K, the orientation of the ClO_4^- alternates in the \mathbf{b} direction and is uniform in the \mathbf{a} and \mathbf{c} directions. This order is thus characterized by the reduced wave vector $\mathbf{q}_2 = (0, 1/2, 0)$.⁸ The alternate order of anions in *stack* direction [for example in $(\text{TMTSF})_2\text{ReO}_4$], occurs at the $2k_F$ critical wave vector of the charge-density-wave (CDW) response of the 1D electronic system. Thus the coupling of the anion ordering (AO) with the $2k_F$ CDW electronic instability ensures that the AO transition leads to a metal-insulator transition with a gap opening associated to a $2k_F$ Peierls-like stack distortion.^{7,9} Thus, in salts with noncentrosymmetric anions, the AO ground state competes with those observed in salts with centrosymmetric anions.

Because of their low electronic dimensionality the instabilities and the phase diagram of the $[\text{TMTS}(\text{T})\text{F}]_2\text{X}$ salts are sizeably affected by the substituents, which can be intro-

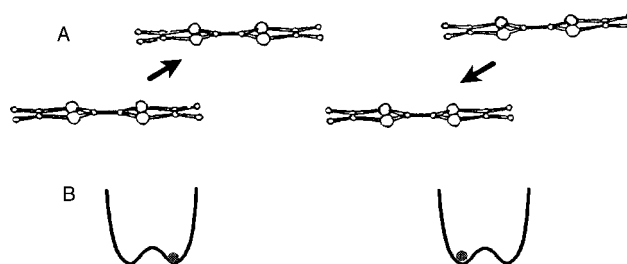


FIG. 1. (a) The two possible orientations of a tetrahedral anion, represented by an arrow, between two neighboring TMTSF molecules and (b) the double well representation of the potential experienced by this anion from its surrounding.

duced either in the organic stacks or in the anion sublattice, and by the disorder resulting of the substitution. Let us mention here some cases studied.

(1) The substitution of the TMTSF by the TMTTF molecule leads to the formation of $[(\text{TMTSF})_{1-x}(\text{TMTTF})_x]_2X$ solid solutions.¹⁰⁻¹³ In the ReO_4 solid solution, nonmonotonic variations with x of the charge transport properties and of the T_{AO} of the \mathbf{q}_1 AO transition are observed.¹³ When x increases from zero in the ClO_4 solid solution, the \mathbf{q}_2 AO transition is rapidly destroyed,¹¹ which leads to a drastic variation with x of the nature of the ground state.¹⁰

(2) Salts of the hybrid TMDTDSF (tetramethyl-diselenadithia-fulvalenium) molecule have been synthesized.^{14(a)} In these salts the noncentrosymmetric TMDTDSF molecule exhibits a random orientational disorder.^{15(a)} The $(\text{TMDTDSF})_2X$ salts show physical properties intermediate between those of $(\text{TMTSF})_2X$ and of $(\text{TMTTF})_2X$. For example, in $(\text{TMDTDSF})_2\text{PF}_6$, spin-peierls (SP) fluctuations, characteristic of $(\text{TMTTF})_2\text{PF}_6$, are observed together with a SDW instability, characteristic of $(\text{TMTSF})_2\text{PF}_6$.^{14,15(b)} $(\text{TMDTDSF})_2\text{ReO}_4$ undergoes a \mathbf{q}_1 AO transition at a critical temperature intermediate between the T_{AO} of $(\text{TMTSF})_2\text{ReO}_4$ and of $(\text{TMTTF})_2\text{ReO}_4$.^{14(b),15(b)} However, because of the disorder in the \mathbf{q}_1 AO transition, observed in $(\text{TMTSF})_2\text{BF}_4$ and in $(\text{TMTTF})_2\text{BF}_4$, is suppressed in $(\text{TMDTDSF})_2\text{BF}_4$.^{15(b)}

(3) By substitution of anions of the same symmetry, $[\text{TMTS}(\text{T})\text{F}]_2X_{1-x}Y_x$ solid solutions can be formed. Among them the $(\text{TMTSF})_2(\text{ReO}_4)_{1-x}(\text{ClO}_4)_x$ solid solution exhibits an interesting succession of different ground states,^{16,17} as for $[(\text{TMTSF})_{1-x}(\text{TMTTF})_x]_2\text{ClO}_4$. For low concentrations of ReO_4^- ($x \approx 1$), it is found that the ambient pressure superconductivity of $(\text{TMTSF})_2\text{ClO}_4$ is rapidly suppressed at the expense of a SDW ground state. In this concentration range, the substitution of the ClO_4^- by the ReO_4^- destroys rapidly the \mathbf{q}_2 AO transition. On the other hand, the study of the ReO_4^- -rich side of the solid solution shows that a substantial substitution ($x=0.35$) of the ReO_4^- by the ClO_4^- preserves the \mathbf{q}_1 AO and keeps the metal-insulator transition.

This paper presents a study of the $(\text{TMTSF})_2(\text{ReO}_4)_{1-x}(\text{ClO}_4)_x$ solid solution, for intermediate x values, for the purpose of determining how the \mathbf{q}_1 AO of pure $(\text{TMTSF})_2\text{ReO}_4$ is replaced by the \mathbf{q}_2 AO of pure $(\text{TMTSF})_2\text{ClO}_4$ and to specify the influence of the AO phase diagram on the electronic properties of the solid solution.

These solid solutions also provide very simple examples of orientational glasses. Previous studies^{15,18} have shown that the AO order parameter can be represented by an Ising variable, η_i , and that depending on the nature of the substituent the disorder can be modelled either by random fields, h_i , acting on η_i , or by random interactions J_{ij} between the Ising variables. The fact that in the $[(\text{TMTSF})_{1-x}(\text{TMTTF})_x]_2X$ and $[\text{TMTS}(\text{T})\text{F}]_2X_{1-x}Y_x$ solid solutions and in the $(\text{TMDTDSF})_2X$ hybrid salts these two types of randomness can be clearly distinguished has a particular relevance to the field of orientational glasses where generally the effects of random fields and of random interactions, both invoked to explain the absence of long range orientational order, cannot be separated.¹⁹ As we shall see in this paper, only the random interactions are present in the

$(\text{TMTSF})_2(\text{ReO}_4)_{1-x}(\text{ClO}_4)_x$ solid solution.

The paper is organized as follows. The experimental conditions and results are given in Secs. II and III, respectively. The structural phase diagram is discussed in Sec. IV and its implications on the electronic properties are outlined in Sec. V.

II. EXPERIMENT

Single crystals, of dimension $6 \times 0.1 \times 0.01 \text{ mm}^3$, of the $(\text{TMTSF})_2(\text{ReO}_4)_{1-x}(\text{ClO}_4)_x$ solid solution were prepared by electrocrystallization. As the relative concentration of ReO_4^- and ClO_4^- anions in crystals showed disparity from the nominal concentration of the solution, the concentration of each single crystal studied was determined by microprobe analysis. The lattice parameters were measured at room temperature (RT) on a four-circle diffractometer using 25 Bragg reflections. The x-ray diffuse scattering experiments were performed using a monochromatic $\text{Cu } K\alpha$ radiation ($\lambda = 1.542 \text{ \AA}$) obtained by (002) reflection of the incident beam on a doubly bent graphite monochromator. Higher resolution studies [$\sim 0.008 \text{ \AA}^{-1}$ half width at half maximum (HWHM)] were achieved on a homemade diffractometer equipped with a position sensitive linear detector and a cryocooler operating in the temperature range 25 K–RT. Lower resolution studies ($\sim 0.015 \text{ \AA}^{-1}$ HWHM) were performed with the fixed-film fixed-crystal method until 9 K. Photographic plates were read either with a Joyce-Loeble microdensitometer or using a computer driven transmission scanner.

III. RESULTS

A. Lattice parameters

Diffraction measurements show that $(\text{TMTSF})_2(\text{ReO}_4)_{1-x}(\text{ClO}_4)_x$ forms a continuous solid solution. Whatever the value of x , a single phase with the triclinic symmetry is observed. The unit cell parameters of the $x=0.53, 0.69, 0.72,$ and 0.85 samples synthesized for this study are given in Table I. This table includes also the lattice parameters of the previously studied $x=0.35$ solid solution²⁰ and of the pure, $x=0$ and 1 , compounds.²¹ Table I shows that, within experimental errors, the lattice parameters vary monotonically with x : $a, b,$ and c decrease while $\alpha, \beta,$ and γ increase for x increasing.

B. Substitutional disorder

In order to characterize the $\text{ReO}_4^-/\text{ClO}_4^-$ substitutional disorder of the solid solution we took x-ray patterns at low temperatures (less than 30 K). At such temperatures the diffuse scattering due to thermal vibrations is negligible and the effects of the intrinsic substitutional disorder are more clearly revealed. One of these x-ray patterns is shown Fig. 2(a) for the $x=0.35$ sample. An intense diffuse scattering is observed near the origin of the reciprocal space. It decreases continuously as the Bragg angle (θ) increases. This decrease is more quantitatively illustrated by the scan shown in Fig. 2(b). Its θ dependence can be accounted for by the standard expression for the monotonic Laue scattering in case of random disorder between species A and B:²²

TABLE I. Triclinic lattice parameters of the $(\text{TMTSF})_2(\text{ReO}_4)_{1-x}(\text{ClO}_4)_x$ solid solution [(*) from Refs. 20 and 21].

x	a (Å)	b (Å)	c (Å)	α (deg)	β (deg)	γ (deg)	V (Å ³)
0.00*	7.284(3)	7.751(1)	13.483(1)	83.23(1)	86.56(2)	70.08(2)	710.5(3)
0.35*	7.28(2)	7.704(4)	13.365(5)	83.83(3)	86.7(1)	70.3(1)	701(2)
0.53(5)	7.269(5)	7.695(4)	13.350(9)	84.13(5)	86.75(5)	70.43(5)	700(13)
0.69(6)	7.261(3)	7.695(3)	13.32(1)	83.96(5)	86.51(5)	70.40(3)	697(9)
0.72(2)	7.271(2)	7.687(3)	13.351(4)	84.15(2)	86.74(2)	70.41(2)	697(6)
0.85(7)	7.271(2)	7.676(8)	13.292(3)	84.35(2)	86.72(2)	70.42(1)	695(4)
1.00*	7.266(1)	7.678(1)	13.275(2)	84.58(1)	86.73(1)	70.43(1)	694.4(2)

$$I(\theta) = Cx(1-x)[f_A(\theta) - f_B(\theta)]^2. \quad (1)$$

In expression (1) f_A and f_B are the form factors of the ReO_4^- and the ClO_4^- anions, x is the concentration of the solid solution (here $x=0.35$) and C is a scale factor. As the anions are approximately in the same orientation in the pure compounds and as the Re-O and Cl-O distances of the ReO_4^- and ClO_4^- anions are close, the contribution of oxygen atoms to the Laue scattering can be neglected. The θ dependence of the intensity of the Laue scattering can thus be accounted for by the square of the difference of atomic form factors of the Re and of the Cl [solid line in Fig. 2(b)]. As the Laue scattering is characteristic of crystals with a random substitutional disorder and as we observe the same monotonic dependence of the diffuse intensity on all the x-ray patterns of

the solid solution, we conclude that the $\text{ReO}_4^-/\text{ClO}_4^-$ substitutional disorder is *random* for all concentrations.

C. Anion ordering effects

Let us now study the influence of this random substitutional disorder on the AO transition of the $(\text{TMTSF})_2(\text{ReO}_4)_{1-x}(\text{ClO}_4)_x$ solid solution.

In order to characterize the AO effects, we measured the following quantities:

(a) The critical wave vector \mathbf{q} of the AO from the relative position of the satellite reflections (diffuse spots) with respect to the main Bragg reflections.

(b) The half width at half maximum (HWHM) of the profile around \mathbf{q} at low temperature ($T < 30$ K) in the \mathbf{s} direction, $\Delta_s(\mathbf{q})$. $\Delta_s(\mathbf{q})$ given in this paper is corrected from the experimental resolution, taken as the HWHM of a close Bragg reflection. The scattering whose HWHM is the same as the experimental resolution [$\Delta_s(\mathbf{q})$ equal to zero] are called satellite reflections. In that case, the anions are long-range ordered (LRO) at the scale of our resolution ($\xi \geq 200$ Å).²³ If this is not the case, the anions are short range ordered (SRO) at low temperature. The inverse of $\Delta_s(\mathbf{q})$ measures the *range* of the order. These aspects will be clarified at the end of this section.

(c) The temperature dependence of the peak intensity of the satellite reflection (diffuse spot). In the case of a LRO, this intensity is proportional to the square of the *order parameter*. In order to compare different solid solutions the intensity was normalized (when possible) to its low temperature saturation value.

(d) The thermal dependence of the HWHM of the satellite reflection (diffuse spot). We define the temperature at which the HWHM deviates from its low temperature saturation value as the transition (T_{AO}) or the quasitransition temperature (T'_{AO}) depending on whether a LRO or a SRO is observed at low temperature.

All the results are summarized in Table II, which also includes a more detailed analysis of the data of the ClO_4^- rich side of the solid solution shortly published in Ref. 17.

In the x-ray patterns of the ReO_4^- -rich side of the solid solution, AO satellite reflections or diffuse spots are observed at the $\mathbf{q}_1 = (\frac{1}{2}, \frac{1}{2}, \frac{1}{2})$ reduced wave vector [Fig. 2(a)]. Figure 3 gives the temperature dependence of their intensity for the $x=0, 0.35, 0.53, 0.69,$ and 0.72 samples. For $0 \leq x < 0.53$, the HWHM of the \mathbf{q}_1 satellite reflections reaches the experimental resolution, which means that a LRO of the an-

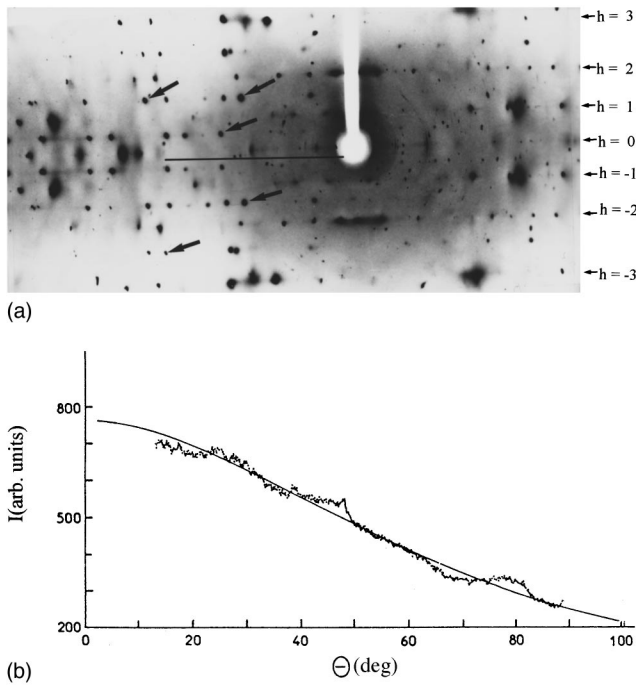


FIG. 2. (a) Fixed-film fixed-crystal x-ray pattern of the $x=0.35$ alloy at 25 K. Layers of Bragg reflections perpendicular to \mathbf{a} are labeled by their Miller indice h . The arrows show the $\mathbf{q}_1 = (\frac{1}{2}, \frac{1}{2}, \frac{1}{2})$ satellite reflections. The continuous line indicates the scan performed in (b). (b) Intensity versus Bragg angle along the scan direction shown in (a). The full line is a fit of the monotonic Laue scattering intensity by expression (1).

TABLE II. Summary of the structural results of the $(\text{TMTSF})_2(\text{ReO}_4)_{1-x}(\text{ClO}_4)_x$ solid solution [(*) from Ref. 17; (**) from Ref. 36 is slowly cooled samples]. T_{AO} (T'_{AO}) is the anion ordering transition (quasitransition) critical temperature and $\Delta_a(\mathbf{q})$ is the HWHM of the diffuse spot in the \mathbf{a} direction, corrected by the experimental resolution.

x	Expt. method	T_{min} (K) reached	T_{AO} (K) (\mathbf{q}_1)	T'_{AO} (K) (\mathbf{q}_1)	T'_{AO} (K) (\mathbf{q}_2)	T_{AO} (K) (\mathbf{q}_2)	$\Delta_a(\mathbf{q}_1)$ (\AA^{-1})	$\Delta_a(\mathbf{q}_2)$ (\AA^{-1})
0.00	Detector	25	176.0(5)				0.000(8)	
0.35	Detector	25	109.0(5)				0.000(8)	
0.53(5)	Detector	25		92.0(5)			0.004(8)	
0.69(6)	Detector	25		57(2)			0.036(8)	
0.72(2)	Fixed-film	18		30(10)	0(18)		0.066(9)	0.094(4)
0.85(7)	Fixed-film	18		0(18)	20(3)		0.075(9)	0.080(9)
0.93*	Fixed-film	18		0(18)	23(1)		0.079(9)	0.034(7)
0.95*					22.5(10)			0.026(7)
0.97*						23(1)		0.00(1)
0.99*						22(1)		0.00(1)
1.00*						24.0(5)		0.002**

ions is established at the scale of our resolution. Figure 3 shows that their intensity vanishes at a T_{AO} which decreases when x increases. A slight broadening of the HWHM, with respect to the experimental resolution, begins to be observed for the $x=0.53$ sample (Fig. 4). For larger x values, going until about $x=0.93$, \mathbf{q}_1 diffuse spots broader than the experimental resolution are detected (SRO of the anions); see Figs. 5 and 6 for the $x=0.69$ and $x=0.72$ samples, respectively. T'_{AO} , their quasitransition temperature, defined by the temperature of saturation of the HWHM of the diffuse spots [see Fig. 7(a) for $x=0.72$], decreases also when x increases. Very weak and broad \mathbf{q}_1 diffuse spots, whose HWHM does not seem to saturate at low temperature, are observed for x larger than 0.72. For $x>0.93$ the \mathbf{q}_1 diffuse spots are no longer detected.

The ClO_4^- -rich side of the solid solution ($0.93 \leq x \leq 1$) was previously investigated in Ref. 17. This work showed,

for $0.97 \leq x \leq 1$, a $\mathbf{q}_2 = (0, \frac{1}{2}, 0)$ LRO of the anions (at the scale of our experimental resolution). The \mathbf{q}_2 reflections exhibited a rapid broadening for $x < 0.97$ (\mathbf{q}_2 SRO). Our work shows that broad \mathbf{q}_2 diffuse spots are still observed in the $x=0.85$ and $x=0.72$ samples (Fig. 6). They are no longer detected in the $x=0.69$ sample (Fig. 5). Surprisingly it is found (Table II) that, within experimental errors, the \mathbf{q}_2 transition (T_{AO}) or quasitransition (T'_{AO}) temperature remains constant with x .

The x-ray pattern of the $x=0.72$ alloy shows a coexistence of the \mathbf{q}_1 and \mathbf{q}_2 local orders (Fig. 6). Figures 7(a) and 7(b) give the temperature dependence of the peak intensity and of the HWHM of the \mathbf{q}_1 and \mathbf{q}_2 diffuse spots, respectively. It shows that the HWHM of the \mathbf{q}_1 diffuse spot saturates at a value larger than the experimental resolution and that the HWHM of the \mathbf{q}_2 diffuse spot does not seem to

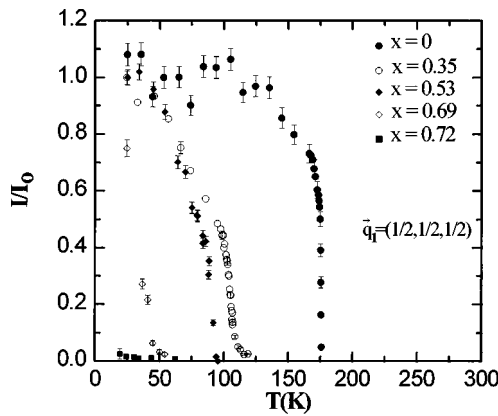


FIG. 3. Temperature dependence of the \mathbf{q}_1 satellite (diffuse spot) intensity of the $(\text{TMTSF})_2(\text{ReO}_4)_{1-x}(\text{ClO}_4)_x$ solid solution for $x=0, 0.35, 0.53, 0.69$, and 0.72 . The intensity is normalized at its saturation value, except for the $x=0.69$ and 0.72 samples where the intensity does not saturate at low temperature. For $x=0, 0.35, 0.53$, and 0.69 the integrated intensity was measured with a position sensitive linear detector. For $x=0.72$ the intensity was obtained from microdensitometer readings of x-ray patterns.

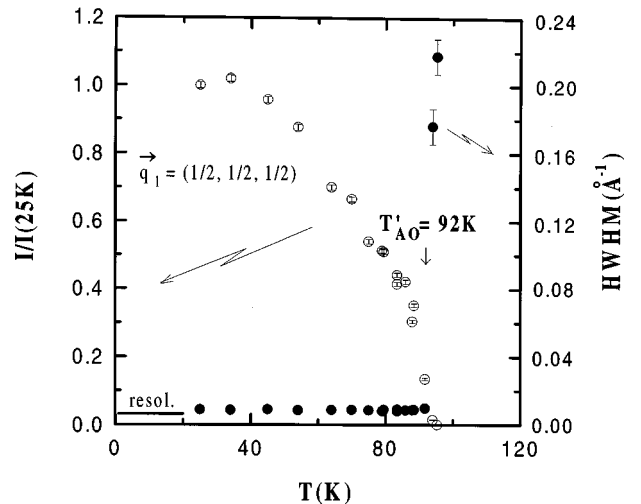


FIG. 4. Temperature dependence of the normalized intensity and of the HWHM along \mathbf{a} of a \mathbf{q}_1 satellite of $(\text{TMTSF})_2(\text{ReO}_4)_{0.47}(\text{ClO}_4)_{0.53}$. T'_{AO} is the temperature at which there is a broadening of the satellite reflection together with a drop of its intensity.

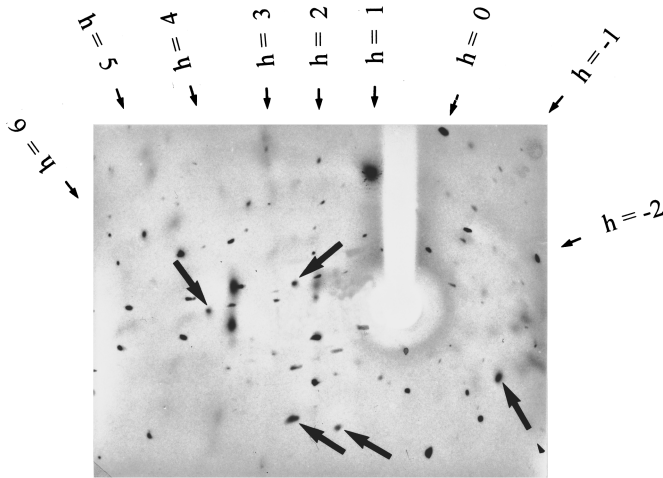


FIG. 5. X-ray pattern of $(\text{TMTSF})_2(\text{ReO}_4)_{0.31}(\text{ClO}_4)_{0.69}$ at 9 K. The arrows show the $\mathbf{q}_1 = (\frac{1}{2}, \frac{1}{2}, \frac{1}{2})$ diffuse spots. The layers of main Bragg reflections perpendicular to \mathbf{a} are labeled by their Miller index h .

saturate at low temperature. The coexistence of the \mathbf{q}_1 and \mathbf{q}_2 SRO is also observed in the $x=0.85$ and 0.93 samples.

Figure 8, obtained from the data of Table II, gives the concentration dependence of $\Delta_a(\mathbf{q}_1)$ and $\Delta_a(\mathbf{q}_2)$ determined at $T < 30$ K. Within experimental errors $\Delta_a(\mathbf{q}_1)$ is zero until about $x \approx 0.5$. For $x > 0.6$, $\Delta_a(\mathbf{q}_1)$ increases rapidly and saturates at about 0.08 \AA^{-1} above $x \approx 0.7$. On the other hand, $\Delta_a(\mathbf{q}_2)$ is zero in a very small range of concentration, $0.97 \leq x \leq 1$. For $x < 0.97$, $\Delta_a(\mathbf{q}_2)$ increases rapidly and saturates at about 0.09 \AA^{-1} below $x \approx 0.85$. The \mathbf{q}_1 LRO, which persists until about $x \approx 0.5$, is rapidly destroyed for x larger than 0.6 , probably because of the competition with the \mathbf{q}_2 SRO. Note that $\Delta_a(\mathbf{q}_1)$ saturates when the \mathbf{q}_2 SRO is present. $\Delta_a(\mathbf{q}_1)$ becomes larger than $\Delta_a(\mathbf{q}_2)$ for $x \geq 0.85$. When the \mathbf{q}_1 SRO vanishes, $\Delta_a(\mathbf{q}_2)$ rapidly decreases. The \mathbf{q}_2 LRO is observed for $x \geq 0.97$.

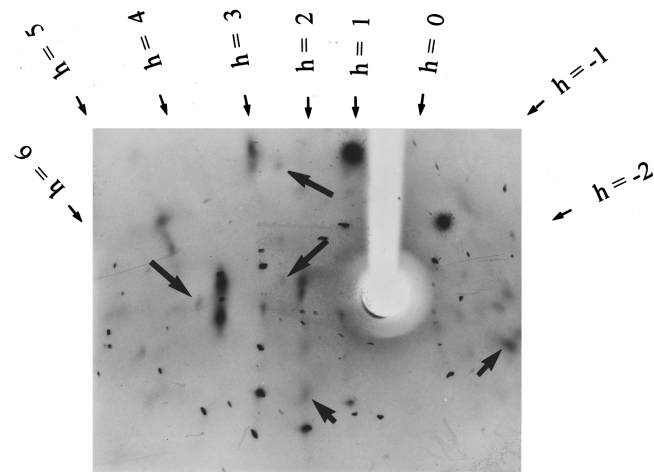


FIG. 6. X-ray pattern of $(\text{TMTSF})_2(\text{ReO}_4)_{0.28}(\text{ClO}_4)_{0.72}$ at 24 K. The diffuse spots at $\mathbf{q}_1 = (\frac{1}{2}, \frac{1}{2}, \frac{1}{2})$ and $\mathbf{q}_2 = (0, \frac{1}{2}, 0)$ are shown by long and short arrows, respectively. The layers of main Bragg reflections perpendicular to \mathbf{a} are labeled by their Miller index h . This x-ray pattern is taken with about the same orientation as that of Fig. 5. Note the net decrease of the intensity of the \mathbf{q}_1 diffuse spots between Figs. 5 and 6.

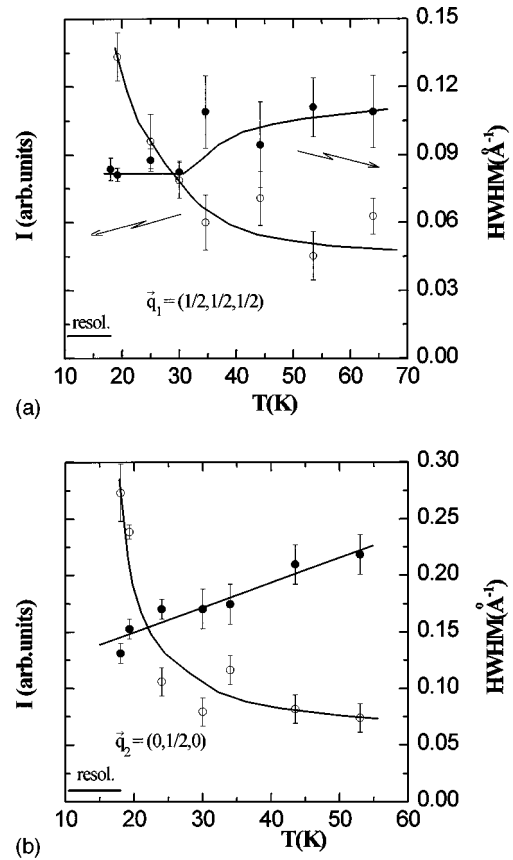


FIG. 7. Temperature dependence of the peak intensity (empty symbols) and of the HWHM along the \mathbf{a} direction (full symbols) of the \mathbf{q}_1 (a) and \mathbf{q}_2 (b) diffuse spots of $(\text{TMTSF})_2(\text{ReO}_4)_{0.28}(\text{ClO}_4)_{0.72}$. In (a) T'_{AO} is the temperature below which the HWHM of the \mathbf{q}_1 diffuse spots saturates. Such a saturation not being observed in (b), an upper limit at the T'_{AO} of the \mathbf{q}_2 scattering is 18 K. The continuous lines are a guide for the eyes.

Figure 9 summarizes all the results obtained by structural and conductivity measurements in a diagram giving T_{AO} or T'_{AO} in function of the ClO_4^- concentration, x . It shows that within experimental errors T_{AO} and T'_{AO} of the \mathbf{q}_1 AO linearly decreases when x increases until about 0.7 and that above this concentration T'_{AO} abruptly vanishes. Contrarily, T_{AO} and T'_{AO} of the \mathbf{q}_2 AO remains constant when x decreases from 1 until about 0.85 . Below this concentration, T'_{AO} vanishes.

Another important quantity which characterizes the nature of the SRO is the profile of diffuse spots, i.e., the \mathbf{q} dependence of their intensity. Figure 10 shows the profile along \mathbf{a}

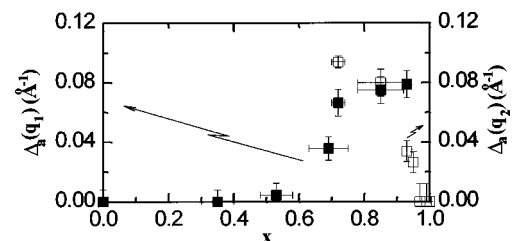


FIG. 8. Concentration dependence (x) of the intrinsic HWHM along \mathbf{a} of the \mathbf{q}_1 (full symbols, left scale) and \mathbf{q}_2 (empty symbols, right scale) diffuse spots at low temperature ($T < 30$ K).

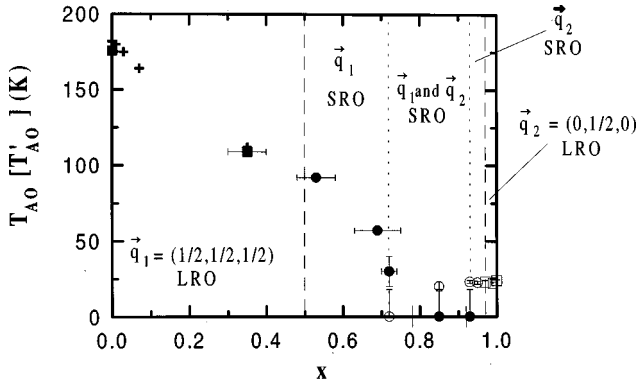


FIG. 9. Concentration dependence (x) of the AO transition temperature (T_{AO}) and of the quasitransition temperature (T'_{AO}) determined by structural measurements. The full symbols represent the \mathbf{q}_1 order and the empty ones the \mathbf{q}_2 order. The LRO (squares) or SRO (circles) nature of the \mathbf{q}_1 and \mathbf{q}_2 AO ground states is also indicated. T_{AO} obtained by the conductivity measurements of Ref. 20 are represented by crosses.

of a \mathbf{q}_1 diffuse spot of the $(\text{TMTSF})_2(\text{ReO}_4)_{0.31}(\text{ClO}_4)_{0.69}$ solid solution. In this sample, where the HWHM is much larger than the HWHM of the resolution, the profile can be fitted by a Lorentzian square function. A Lorentzian square profile is also observed along \mathbf{a} for the \mathbf{q}_2 diffuse spots of $(\text{TMTSF})_2(\text{ReO}_4)_{0.07}(\text{ClO}_4)_{0.93}$.²⁴ As a Lorentzian square function has a \mathbf{q} dependence intermediate between a Lorentzian and a Gaussian, and as our resolution has a Gaussian shape, we have taken, in Table II and in Fig. 8, $\Delta_a(\mathbf{q})$ as the mean value of the intrinsic $\Delta_a(\mathbf{q})$ obtained from the Lorentzian-Gaussian and Gaussian-Gaussian resolution corrections.

IV. DISCUSSION

In $(\text{TMTTF})_2X$ and $(\text{TMTSF})_2X$ salts, each anion is located between two S(Se) identical atoms. Its environment can be schematically represented by a symmetric double well potential [Fig. 1(b)]. Each anion (located in i) can occupy one of the two minima of this potential. The orientation of a

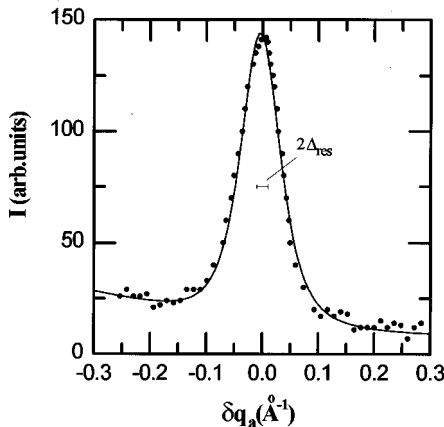


FIG. 10. Profile along \mathbf{a} of a \mathbf{q}_1 diffuse spot of $(\text{TMTSF})_2(\text{ReO}_4)_{0.31}(\text{ClO}_4)_{0.69}$ at 9 K and its fit (continuous line) by a Lorentzian square profile. The FWHM of the experimental resolution ($2\Delta_{\text{res}}$) is indicated.

given anion is thus specified by the Ising variable η_i , which can be taken as the order parameter; $\eta_i = \pm 1$ if the anion points towards the Se atom of the left/right side neighboring TMTSF molecule.

The coupling between anions, leading to the AO transition, can be described by the phenomenological Hamiltonian:

$$H = \sum_{i,j} J_{ij} \eta_i \eta_j, \quad (2)$$

where J_{ij} is the interaction between two anions located in i and j . In pure $(\text{TMTSF})_2\text{ReO}_4$, the “ J_{ij} ” are such that the alternate order of the ReO_4^- anions in the three directions [$\mathbf{q}_1 = (\frac{1}{2}, \frac{1}{2}, \frac{1}{2})$] is stabilized below $T_{AO} = 176$ K. In pure $(\text{TMTSF})_2\text{ClO}_4$, the “ J_{ij} ” are such that the uniform order of ClO_4^- anions along \mathbf{a} and \mathbf{c} , and the alternate order along \mathbf{b} [$\mathbf{q}_2 = (0, \frac{1}{2}, 0)$] is stabilized below $T_{AO} = 24$ K.

In the case of a random disorder of TMTSF and TMTTF organic molecules, in $[(\text{TMTSF})_{1-x}(\text{TMTTF})_x]_2X$ solid solutions, and in the case of a random orientational disorder of TMDTDSF molecules, in $(\text{TMDTDSF})_2X$ salts, the anions can be in S-symmetric, Se-symmetric, or S-Se asymmetric potentials which are randomly distributed all over the anion positions. In the S-Se environment, the anions thus experience an asymmetric double well potential which breaks the ± 1 symmetry of the order parameter. This effect can be modeled by the presence of a local field h_i coupled to η_i . The AO process thus occurs in the presence of *random fields*. On the other hand in $(\text{TMTSF})_2X_{1-x}Y_x$ solid solutions the X(Y) anions remain located between two Se atoms. Random fields effects are thus not present. But, if the interaction J_{ij} between the Ising variables η_i and η_j depends of the nature X or Y of the anions located in i and j , the random substitution of anions introduces random interactions J_{ij} .

The observation of the Laue monotonic scattering in the $(\text{TMTSF})_2(\text{ReO}_4)_{1-x}(\text{ClO}_4)_x$ solid solution shows that there is a random substitution of the anions. As the critical wave vector of the AO transition of $(\text{TMTSF})_2\text{ReO}_4(\mathbf{q}_1)$ and of $(\text{TMTSF})_2\text{ClO}_4(\mathbf{q}_2)$ is different, it is expected quite important random interactions. We will thus discuss the phase diagram of the solid solution within the framework of the Ising model, described by the Hamiltonian (2), with random interactions J_{ij} .

This random interaction model has already been used by Sherrington and Kirkpatrick²⁵ to derive the phase diagram of spin glasses in the case where the interactions J_{ij} are infinitely ranged and where their distribution follows a Gaussian law defined by a mean interaction $\langle J \rangle$ and a standard deviation ΔJ . Their treatment shows that for $\langle J \rangle > (\Delta J)$, the system undergoes a phase transition at $\langle J \rangle / k_B$, and for $\langle J \rangle < (\Delta J)$, the system undergoes a glass transition at $\Delta J / k_B$.

This theory was used to interpret the phase diagram of the mixed ferroelectric-antiferroelectric solid solution: $\text{Rb}_{1-x}(\text{NH}_4)_x\text{H}_2\text{PO}_4$ (RADP) and $\text{Rb}_{1-x}(\text{NH}_4)_x\text{H}_2\text{AsO}_4$ (RADA).²⁶ In the case of a competition between the $-J$ (“ferro”) coupling and the $+J$ (“antiferro”) coupling between z first neighbors, the mean field theory shows,²⁷ similar to the results of Sherrington and Kirkpatrick, that for $\sqrt{z}|\langle J \rangle| > \Delta J$, there is a phase transition to a ferroelectric or

antiferroelectric order at $|\langle J \rangle|z/k_B$, depending if $\langle J \rangle < 0$ or if $\langle J \rangle > 0$, and for $\sqrt{z}|\langle J \rangle| < \Delta J$, there is a glass transition at $\Delta J\sqrt{z}/k_B$.

In these last expressions one has, if the probability of the $+J(-J)$ coupling is $1-x(+x)$,

$$\langle J \rangle = (1-2x)J, \quad (3)$$

$$\Delta J = 2J\sqrt{x(1-x)}. \quad (4)$$

In the following we will apply the results of such mean field models to an *oversimplified* description of the $(\text{TMTSF})_2(\text{ReO}_4)_{1-x}(\text{ClO}_4)_x$ solid solution. We define J_1 , J_2 , and J_3 as the interaction between two ReO_4^- anions, two ClO_4^- anions, one ReO_4^- anion, and one ClO_4^- anion, respectively. We shall assume that this interaction is the same in all the crystallographic directions, which is not too bad an approximation because the AO pretransitional fluctuations of the $(\text{TMTSF})_2\text{ReO}_4$ (Ref. 28) and $(\text{TMTSF})_2\text{ClO}_4$ (Ref. 29) transitions are roughly isotropic. The probability of such interactions are, respectively, $p(J_1) = (1-x)^2$, $p(J_2) = x^2$, and $p(J_3) = 2x(1-x)$, if x is the concentration of ClO_4^- in the solid solution. The average interaction is

$$\langle J \rangle = \sum_i p(J_i)J_i, \quad (5)$$

$$\langle J \rangle = (1-x)J_1 + xJ_2,$$

if J_3 is taken as the mean value of the J_1 and J_2 . With the same assumptions the standard deviation is given by

$$\Delta J = \sqrt{\sum_i p(J_i)(J_i - \langle J \rangle)^2}, \quad (6)$$

$$\Delta J = \sqrt{x(1-x)/2}|J_2 - J_1|.$$

In order to calculate $\langle J \rangle$ and (ΔJ) , we shall take

$$T_{\text{AO}}^1 = |J_1|/k_B = 176 \text{ K},$$

$$T_{\text{AO}}^2 = |J_2|/k_B = 24 \text{ K},$$

and we shall assume, as the ReO_4^- and ClO_4^- anions take opposite orientations in the **a** and **c** directions, that J_1 and J_2 have opposite signs. This gives

$$\langle J \rangle/k_B = -24x + 176(1-x), \quad (7)$$

$$\Delta J/k_B = 200\sqrt{x(1-x)}/2. \quad (8)$$

These two quantities are represented in function of x in Fig. 11. It is found that $|\langle J \rangle|$ is superior to $|\Delta J|$ for $0 \leq x \leq 0.53$ and $0.97 \leq x \leq 1$. In these concentration ranges the infinitely ranged model thus predicts a LRO at $T_{\text{AO}} \sim |\langle J \rangle|/k_B$. It is found that $|\Delta J|$ dominates $|\langle J \rangle|$ for $0.53 < x < 0.97$. In this concentration range the infinitely ranged model thus predicts an ‘‘orientational glass’’ phase below $T_G \sim |\Delta J|/k_B$ (i.e., T'_{AO} below). This model predicts quite well the concentration ranges where the LRO and SRO are observed. It predicts also quite well the concentration dependence of T_{AO} and T'_{AO} in the ReO_4^- rich side of the solid

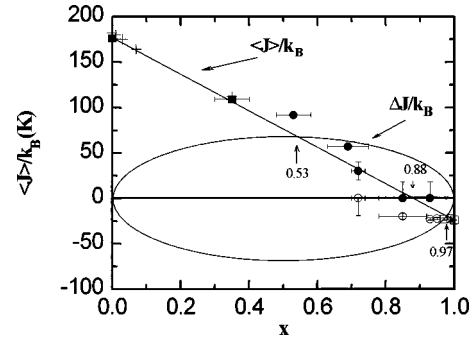


FIG. 11. Comparison of the experimental phase (T,x) diagram with that predicted by the infinitely ranged random interaction Ising model described in the text. The data are reported with the same symbols as in Fig. 9. The temperatures are taken positive for the \mathbf{q}_1 AO and negative for the \mathbf{q}_2 AO. The continuous lines represent $\langle J \rangle/k_B$ and $\Delta J/k_B$, given, respectively, by expressions (7) and (8).

solution. But the behavior of T'_{AO} is not well reproduced in the concentration range, $0.7 < x < 0.95$, where the main critical AO wave vector shifts from \mathbf{q}_1 to \mathbf{q}_2 .

This very simple model does not take into account the \mathbf{q} dependence of the instabilities. It implicitly assumes that the main instabilities appear at the \mathbf{q}_1 and \mathbf{q}_2 wave vectors. In this respect, the competing aspect of the instabilities is not taken well into account. A better approach would be to explicitly calculate the instantaneous correlation function,

$$S(\mathbf{q}) = \langle |\eta_{\mathbf{q}}|^2 \rangle, \quad (9)$$

actually measured in our x-ray diffuse scattering experiments, where $\eta_{\mathbf{q}}$ is the Fourier transform of the Ising variable η_i . In the classical limit one has

$$S(\mathbf{q}) = k_B T \chi(\mathbf{q}), \quad (10)$$

where $\chi(\mathbf{q})$ is the generalized susceptibility.

Let us first calculate the inverse of this quantity in the case of the Ising model already introduced. For the Hamiltonian (2) the mean field approximation gives

$$\chi^{-1}(\mathbf{q}) = k_B T + J(\mathbf{q}), \quad (11)$$

where $J(\mathbf{q})$ is the Fourier transform of the interaction $J_{ij} = J_{j-i}$, between anions at sites 0 and $j-i$. Explicitly, this quantity reads

$$J(\mathbf{q}) = 2[J_a^\alpha \cos \mathbf{q}\mathbf{a} + J_b^\alpha \cos \mathbf{q}\mathbf{b} + J_{a-b}^\alpha \cos \mathbf{q}(\mathbf{a}-\mathbf{b}) + J_c^\alpha \cos \mathbf{q}\mathbf{c}], \quad (12)$$

where the J_a^α are the interaction between anions of type $\alpha = 1, 2$ (ReO_4^- and ClO_4^-) in the **u** directions (**a**, **b**, **a-b**, or **c**) of first neighbors.

In the framework of the above-mentioned discussion, the average interaction in the solid solution can be written

$$\langle J(\mathbf{q}) \rangle = 2\{[(1-x)J_a^1 + xJ_a^2] \cos \mathbf{q}\mathbf{a} + [(1-x)J_b^1 + xJ_b^2] \cos \mathbf{q}\mathbf{b} + [(1-x)J_{a-b}^1 + xJ_{a-b}^2] \cos \mathbf{q}(\mathbf{a}-\mathbf{b}) + [(1-x)J_c^1 + xJ_c^2] \cos \mathbf{q}\mathbf{c}\}. \quad (13)$$

It is shown in the Appendix that the ratios between the J_u^α can be obtained from the experimental values of the correlation lengths. One gets

$$J_a^1 \approx J_b^1 \approx -2J_{a-b}^1 \approx 2.5J_c^1, \quad \text{with } J_a^1 > 0, \quad \text{for the } \mathbf{q}_1 \text{ AO,}$$

$$J_a^2 \approx -J_b^2 \approx -2J_{a-b}^2 \approx 2.5J_c^2, \quad \text{with } J_a^2 < 0,$$

for the \mathbf{q}_2 AO.

With these values Eq. (13) becomes

$$\begin{aligned} \langle J(\mathbf{q}) \rangle = & 2[xJ_a^2 + (1-x)J_a^1][\cos \mathbf{q}\mathbf{a} - 0.5 \cos \mathbf{q}(\mathbf{a}-\mathbf{b}) \\ & + 0.4 \cos \mathbf{q}\mathbf{c}] - 2[xJ_a^2 - (1-x)J_a^1] \cos \mathbf{q}\mathbf{b}. \end{aligned} \quad (14)$$

If this expression ensures that the maxima of the diffuse scattering will be around \mathbf{q}_1 for $x=0$ and \mathbf{q}_2 for $x=1$, it fails to explain the x dependence of the diffuse scattering. For example, if the last term of the right member of Eq. (14) shows that $J(\mathbf{q})$ is always maximal for $\mathbf{q}_b = \mathbf{b}^*/2$, the \mathbf{q}_a and \mathbf{q}_c components will not be determined when, for $(1-x)J_a^1 + xJ_a^2 = 0$, the first term of this member will vanish. With the J_u^α values estimated in the Appendix this occurs for $x \approx 0.88$, indicating that the solid solution would be disordered at any temperature for this concentration, contrary to the experimental observation of well defined \mathbf{q}_1 and \mathbf{q}_2 diffuse spots around this concentration.

This is a very general feature of any Ising model with competing interactions.³⁰ Depending on the exact values of the interactions, these models usually predict such ‘‘disorder lines’’ [in a generalized phase diagram, like our (x, T) diagram], where the system is more disordered. Disorder lines of different types have been recognized both experimentally and theoretically in systems with competing interactions.^{31,32} Disorder lines are mainly due to a similar expression of the interaction constants $J^\alpha(\mathbf{q})$ ($\alpha=1,2$), all having the same physical origin, and which give rise to a cancellation of the average interaction $\langle J(\mathbf{q}) \rangle$ for a specific x . This feature rules out the possibility of observing both instabilities in certain regions of the phase diagram. This indicates that the Ising model is not appropriate to explain the phase diagram of our solid solutions. Let us remark that this conclusion is at variance with what was proposed for these compounds:³³ the $(\text{TMTSF})_2(\text{ReO}_4)_{1-x}(\text{ClO}_4)_x$ phase diagram does not exhibit any disorder lines, but, as a function of x , a gradual disappearance of the \mathbf{q}_1 AO at the expense of the \mathbf{q}_2 AO.

In an attempt to solve this problem, let us come back to the actual microscopic interactions between anions in our solid solution. Though the exact microscopic constants are not exactly known, a general model of the AO instabilities has already been presented.¹⁶ As previously mentioned, the \mathbf{q}_1 AO is driven by the $2\mathbf{k}_F$ CDW instability of the TMTSF stack. The unstable electronic system is coupled to the phonon mode $u_{\mathbf{q}}$ through the electron-phonon coupling constant. This coupling gives rise to a phonon instability, represented by the phonon susceptibility $\chi_u(\mathbf{q})$, peaked at the $2\mathbf{k}_F$ wave vector. The phonons and the electrons are in turn coupled to the AO order parameter through a general coupling constant $K(\mathbf{q})$. As far as the \mathbf{q}_2 AO is concerned, it is more likely due

to ‘‘direct’’ interactions between the anions, whose interaction constant, $J^2(\mathbf{q})$, is maximum at the \mathbf{q}_2 wave vector previously introduced. With these definitions the free energy of a coupled system of anions and organic chains can be put under the form

$$\begin{aligned} F = & \frac{1}{2} \sum_{\mathbf{q}} [k_B T + J^2(\mathbf{q})] \eta_{\mathbf{q}} \eta_{-\mathbf{q}} + \sum_{\mathbf{q}} K(\mathbf{q}) \eta_{\mathbf{q}} u_{-\mathbf{q}} \\ & + \frac{1}{2} \sum_{\mathbf{q}} \chi_u(\mathbf{q})^{-1} u_{\mathbf{q}} u_{-\mathbf{q}}. \end{aligned} \quad (15)$$

Minimizing F with respect to $u_{\mathbf{q}}$ yields

$$F = \frac{1}{2} \sum_{\mathbf{q}} [k_B T + J^2(\mathbf{q}) - K(\mathbf{q})^2 \chi_u(\mathbf{q})] \eta_{\mathbf{q}} \eta_{-\mathbf{q}} \quad (16)$$

and thus

$$\chi^{-1}(\mathbf{q}) = k_B T + J^2(\mathbf{q}) - K(\mathbf{q})^2 \chi_u(\mathbf{q}), \quad (17)$$

which inversely enters in expression (10). This clearly shows the mechanism of the competition between the \mathbf{q}_1 and \mathbf{q}_2 instabilities. It is due to the relative weight of the ‘‘direct’’ interaction between anions, $J^2(\mathbf{q})$, which dominates in the ClO_4 rich side of the phase diagram, and of the mediated interaction through the organic stack, $K(\mathbf{q})^2 \chi_u(\mathbf{q})$, which is stronger in the ReO_4 rich side. Due to the different physical origin of these interactions, their \mathbf{q} dependence does not cancel at a specific x , as in the Ising model. The \mathbf{q}_1 and \mathbf{q}_2 instabilities are now well separated in the Fourier space, as required to neglect instabilities at other wave vectors. This model also allows us to observe a region of coexistence of both instabilities. The key point is that the microscopic competing interactions between anions cannot cancel out anymore for special values of the concentration, as the Ising model predicts.

This mechanism allows us also to simply explain why the T'_{AO} of the \mathbf{q}_1 SRO abruptly vanishes around $x \approx 0.7$. The reason is that $\chi_u(2\mathbf{k}_F)$, measured in $(\text{TMTSF})_2\text{PF}_6$ for example,²⁴ decreases below 50 K and vanishes below 20 K. Thus the effective coupling constant $K(\mathbf{q})^2 \chi_u(\mathbf{q})$, which drops below 50 K, will not remain important enough to stabilize a \mathbf{q}_1 quasitransition at low temperature.

The observation of a Lorentzian squared profile for the \mathbf{q}_1 and \mathbf{q}_2 diffuse spots in the intermediate concentration range could be explained by a random distribution of domain sizes³⁴ due to the competing interactions previously considered. If κ is the (constant) probability to cross a domain wall per unit length, the probability that two sites, separated by a distance r , belong to the same domain is given by³⁵

$$G(r) = \exp(-\kappa r). \quad (18)$$

Its 3D Fourier transform, performed in a diffraction experiment, is a Lorentzian square function (assuming an isotropic probability κ):

$$S(\mathbf{q}) = \frac{1}{[\kappa^2 + \delta q^2]^2}. \quad (19)$$

Such a profile can account for the shape of the \mathbf{q}_1 (Fig. 10) and \mathbf{q}_2 (Ref. 24) diffuse spots in the SRO regime. In that case, the HWHM (Table II) of the diffuse spot, $\Delta(q)$, is related to κ by

$$\Delta(q) = \kappa \sqrt{\sqrt{2} - 1} \approx 0.64\kappa. \quad (20)$$

V. CONCLUDING REMARKS

In this paper we mainly considered the structural aspects of the AO transition in the $(\text{TMTSF})_2(\text{ReO}_4)_{1-x}(\text{ClO}_4)_x$ solid solution. Such features have important consequences for the instabilities and the quasi-1D electronic properties of the TMTSF stacks.

For x lower than 0.7, a \mathbf{q}_1 AO, and thus a $2\mathbf{k}_F$ CDW modulation of the organic stacks, occurs in domains whose size increases when x decreases (see Fig. 8). At the scale of our experimental resolution a \mathbf{q}_1 LRO is achieved for x lower than 0.5. The stabilization of a long range $2\mathbf{k}_F$ periodicity, and thus a CDW distortion of the TMTSF stacks, opens a well defined energy gap, which has been clearly detected in the $x=0.35$ compound.¹⁶

On the other hand, in the ClO_4^- rich side of the solid solution, the establishment of a \mathbf{q}_2 SRO, for $x < 0.97$, suppresses the superconductivity and stabilizes the $2\mathbf{k}_F$ SDW ground state.¹⁶ In this concentration range the effect of ReO_4^- alloying appears to be similar to the quench of the \mathbf{q}_2 AO transition in pure $(\text{TMTSF})_2\text{ClO}_4$ where it has been observed that, with the reduction of the fraction and of the size of \mathbf{q}_2 ordered domains, when the cooling rate increases,³⁶ the superconductivity is destabilized at the benefit of the SDW ground state.¹ In these systems the superconductivity occurs in the presence of a \mathbf{q}_2 LRO which leads to a splitting by $\Delta\mathbf{k}_F$ of the Fermi wave vector, and thus prevents the stabilization of a density wave ground state by nesting of the Fermi Surface (FS). However, it has recently been suggested²⁴ that the nesting mechanism will still be operating if the \mathbf{q}_2 AO occurs in small enough domains so that $\Delta\mathbf{k}_F$ will be less than $\Delta_a(\mathbf{q}_2)$. A restoration of the nesting properties of the FS, by setting a \mathbf{q}_2 SRO, will thus stabilize the $2\mathbf{k}_F$ SDW ground state. In agreement with this interpretation, Fig. 8 and Table II show that $\Delta_a(\mathbf{q}_2)$ rapidly increases in the same concentration range, x lower than 0.97, where the SDW ground state is observed.

It is not known how the $2\mathbf{k}_F$ SDW ground state evolves when the ReO_4^- content increases further. The study of the solid solution could be especially interesting when, for $0.7 < x < 0.94$, the \mathbf{q}_1 SRO also becomes stable at low temperature and coexists with the \mathbf{q}_2 SRO. In this interesting concentration range the $2\mathbf{k}_F$ SDW and $2\mathbf{k}_F$ CDW orders could locally coexist in the \mathbf{q}_2 and \mathbf{q}_1 domains, respectively. As the $2\mathbf{k}_F$ CDW and $2\mathbf{k}_F$ SDW differ by the relative phase shift θ between the spin- \uparrow and spin- \downarrow electronic densities, $\rho_\uparrow(x)$ and $\rho_\downarrow(x)$ ($\theta=0$ for a CDW, $\theta=\pi$ for a SDW), it is possible, as schematically shown in Fig. 12, that the change of nature of the density wave ground state, between the \mathbf{q}_1 and \mathbf{q}_2 domains, could be simply achieved by a spatial variation of θ between well established electronic modulations of opposite spin. Since it has recently been observed²⁴ that the SDW ground state of the $(\text{TMTSF})_2\text{PF}_6$ already presents a mixed

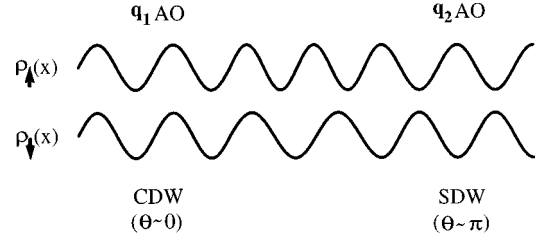


FIG. 12. Schematic representation of the spatial dependence of $\rho_\uparrow(x)$ and $\rho_\downarrow(x)$ on passing from a CDW/ \mathbf{q}_1 AO domain to a SDW/ \mathbf{q}_2 AO domain.

$2\mathbf{k}_F$ CDW/SDW electronic character, such a spatial variation of θ between the \mathbf{q}_1 and \mathbf{q}_2 domains of the solid solution could be less than π . Transport and magnetic measurements should be performed in this interesting concentration range of the $(\text{TMTSF})_2(\text{ReO}_4)_{1-x}(\text{ClO}_4)_x$ solid solution in order to clarify the nature of the ground state in relationship with the structural measurements.

ACKNOWLEDGMENTS

This work has benefited from useful discussions with T. Garel, R. Moret, and S. Tomic. A great part of this work has been performed on the experimental setup constructed by P. A. Albouy who is warmly thanked for his cooperation. K. Bechgaard is also thanked for the gift of the $x=0.35$ sample.

APPENDIX

Near the critical wave vector \mathbf{q}_c , we can develop $J(\mathbf{q})$ in function of $\delta\mathbf{q} = \mathbf{q} - \mathbf{q}_c$:

$$J(\mathbf{q}) = J(\mathbf{q}_c) + \frac{1}{2} \delta\mathbf{q} \frac{\overline{\partial^2 J(\mathbf{q})}}{\partial \mathbf{q}^2} \delta\mathbf{q}. \quad (A1)$$

By defining

$$J(\mathbf{q}_c) = -k_B T_c, \quad (A2)$$

Eq. (11) becomes

$$\chi^{-1}(\mathbf{q}) = k_B(T - T_c) [1 + \delta\mathbf{q} \overline{\xi^2} \delta\mathbf{q}], \quad (A3)$$

where

$$\overline{\xi^2} = \frac{1}{2k_B(T - T_c)} \frac{\overline{\partial^2 J(\mathbf{q})}}{\partial \mathbf{q}^2} \quad (A4)$$

is the tensor of the square of the correlation lengths.

With a good approximation, $\overline{\xi^2}$ is isotropic both for the $\mathbf{q}_1 = (\frac{1}{2}, \frac{1}{2}, \frac{1}{2})$ and $\mathbf{q}_2 = (0, \frac{1}{2}, 0)$ AO transitions of

(TMTSF)₂ReO₄ and (TMTSF)₂ClO₄, respectively. Using $J(\mathbf{q})$ given by Eq. (12) and the lattice parameters of Table I, Eq. (A4) leads to

$$J_a^1 \approx J_b^1 \approx -2J_{a-b}^1 \approx 2.5J_c^1, \quad \text{with } J_a^1 > 0, \quad \text{for the } \mathbf{q}_1 \text{ AO,}$$

$$J_a^2 \approx -J_b^2 \approx -2J_{a-b}^2 \approx 2.5J_c^2, \quad \text{with } J_a^2 < 0,$$

for the \mathbf{q}_2 AO.

From Eqs. (12) and (A2) and the experimental transition temperatures, one has

$$T_{\text{AO}}^1 = |J(\mathbf{q}_1)|/k_B = -5.8J_a^1/k_B = 176 \text{ K; i.e.,}$$

$$J_a^1 \sim -30.5 \text{ K,}$$

$$T_{\text{AO}}^2 = |J(\mathbf{q}_2)|/k_B = 5.8J_a^2/k_B = 24 \text{ K; i.e., } J_a^2 \sim 4 \text{ K.}$$

*Present address: Université de Cergy-Pontoise, 5, Mail Gay Lussac-Neuville sur Oise, 95 031 Cergy-Pontoise Cedex, France.

†Present address: Institut des Matériaux de Nantes, 2, rue de la Houssinière, 44072 Nantes Cedex 03, France.

¹T. Ishiguro and K. Yamaji, *Organic Superconductors*, Springer Series in Solid-State Science Vol. 88 (Springer-Verlag, Berlin, 1990).

²*Organic Conductors: Fundamentals and Applications*, edited by J. P. Farges (Dekker, New York, 1994).

³G. Gruner, *Rev. Mod. Phys.* **66**, 1 (1994).

⁴C. Coulon, in *Organic and Inorganic Low Dimensional Crystalline Materials*, Vol. 168 of *NATO Advanced Study Institute, Series B: Physics*, edited by P. Delhaes and M. Drillon (Plenum, New York, 1987).

⁵D. Jerome, in *Organic Conductors: Fundamentals and Applications* (Ref. 2), p. 405.

⁶J. P. Pouget, in *Organic and Inorganic Low Dimensional Crystalline Materials* (Ref. 4), p. 185.

⁷R. Moret, J. P. Pouget, R. Comes, and K. Bechgaard, *Phys. Rev. Lett.* **49**, 1008 (1982).

⁸J. P. Pouget, G. Shirane, K. Bechgaard, and J. M. Fabre, *Phys. Rev. B* **27**, 5203 (1983).

⁹C. S. Jacobsen, H. J. Pedersen, K. Mortensen, G. Rindorf, N. Thorup, J. B. Torrance, and K. Bechgaard, *J. Phys. C* **15**, 2651 (1982).

¹⁰C. Coulon, P. Delhaes, J. Amiel, J. P. Manceau, J. M. Fabre, and L. Giral, *J. Phys. (France)* **43**, 1721 (1982).

¹¹J. P. Pouget, R. Moret, R. Comes, G. Shirane, K. Bechgaard, and J. M. Fabre, *J. Phys. (Paris), Colloq.* **44**, C3-969 (1983).

¹²K. Mortensen and E. M. Engler, *Phys. Rev. B* **29**, 842 (1984).

¹³V. Ilakovac, S. Ravy, J.-P. Pouget, C. Lenoir, K. Boubekour, P. Batail, S. Dolanski Babic, N. Biskup, B. Korin-Hamzic, S. Tomic, and C. Bourbonnais, *Phys. Rev. B* **50**, 7136 (1994); *Synth. Met.* **70**, 7531 (1995).

¹⁴(a) P. Auban, D. Jerome, K. Lestrup, I. Johannsen, and K. Bechgaard, *J. Phys. (France)* **50**, 2727 (1989); (b) B. Gotschy, P. Auban-Senzier, A. Farrall, C. Bourbonnais, D. Jerome, E. Canadell, R. T. Henriques, I. Johannsen, and K. Bechgaard, *J. Phys. I* **2**, 677 (1992).

¹⁵(a) Q. Liu, S. Ravy, J.-P. Pouget, I. Johannsen, and K. Bechgaard, *J. Phys. I* **3**, 803 (1993); (b) **3**, 821 (1993).

¹⁶S. Tomic, D. Jerome, D. Mailly, M. Ribault, and K. Bechgaard, *J.*

Phys. (Paris), Colloq. **44**, C3-1073 (1983); S. Tomic, D. Jerome, and K. Bechgaard, in *Low Dimensional Conductors and Superconductors*, Vol. 155 of *NATO Advanced Study Institute, Series B: Physics*, edited by D. Jerome and L. G. Caron (Plenum, New York, 1987), p. 307.

¹⁷S. Ravy, R. Moret, J. P. Pouget, and R. Comes, *Physica B* **143**, 542 (1986).

¹⁸V. Ilakovac, Q. Liu, S. Ravy, P. A. Albouy, J. P. Pouget, C. Lenoir, P. Batail, I. Johannsen, and K. Bechgaard, *Synth. Met.* **56**, 2372 (1993).

¹⁹V. T. Hochli, K. Knorr, and A. Loidl, *Adv. Phys.* **39**, 405 (1990).

²⁰S. Tomic, Ph.D. thesis, Orsay, 1986.

²¹N. Thorup, G. Rindorf, and H. Soling, *Phys. Scr.* **25**, 868 (1982).

²²A. Guinier, *X-Ray Diffraction in Crystals, Imperfect Crystals and Amorphous Bodies* (Dover, New York, 1994).

²³We estimate that we are able to detect only a broadening in excess of 1/2 of the HWHM of the experimental resolution. The inverse of this value corresponds to about 200 Å.

²⁴J. P. Pouget and S. Ravy, *J. Phys. I* **6**, 1501 (1996).

²⁵D. Sherrington and S. Kirkpatrick, *Phys. Rev. Lett.* **35**, 1792 (1975).

²⁶R. Blinc, *Z. Naturforsch. Teil A* **45a**, 313 (1990).

²⁷V. Dobrosavljevic and R. M. Stratt, *Phys. Rev. B* **36**, 8484 (1987).

²⁸J. P. Pouget, R. Moret, R. Comes, and K. Bechgaard, *J. Phys. (France) Lett.* **42**, L543 (1981).

²⁹R. Moret, J. P. Pouget, R. Comes, and K. Bechgaard, *J. Phys. (France)* **46**, 1521 (1985).

³⁰T. Garel and J. M. Maillard, *J. Phys. C* **19**, L505 (1986).

³¹T. Garel, V. Ilakovac, and S. Ravy, *Phys. Rev. B* **49**, 12 791 (1994).

³²V. Ilakovac, S. Ravy, A. Moradpour, L. Firlej, and P. Bernier, *Phys. Rev. B* **52**, 4108 (1995).

³³R. Bruinsma and V. J. Emery, *J. Phys. (Paris), Colloq.* **44**, C3-1115 (1983).

³⁴P. Debye, M. R. Anderson, and M. Brumberger, *J. Appl. Phys.* **28**, 679 (1957).

³⁵J. P. Pouget, in *Neutron and Synchrotron Radiation For Condensed Matter Studies*, edited by J. Baruchel, J. L. Hodeau, M. S. Lehmann, J. R. Regnard, and C. Schlenker (Les Editions de Physique) (Springer-Verlag, Berlin, 1994), Vol. II, Chap. XI.

³⁶J. P. Pouget, S. Kagoshima, T. Tamegai, V. Nogami, K. Kubo, T. Nakajima, and K. Bechgaard, *J. Phys. Soc. Jpn.* **59**, 2036 (1990).